Supporting Information

Robust spring-like lamellar VO/C nanostructure for high-rate and long-life potassium-ion batteries

Jian Lu,‡[a] Changlai Wang,‡[ab] Guoliang Xia,[a] Huigang Tong,[a] Yang Yang,[a] Dequan Zhu,[d] and Qianwang Chen*[ac]

[a] Hefei National Laboratory for Physical Science at Microscale, Department of Materials Science and Engineering, University of Science and Technology of China, Hefei, Anhui 230026, P. R. China

[b] Center of Super-Diamond and Advanced Films (COSDAF), Department of Materials Science and Engineering, City University of Hong Kong, Tat Chee Avenue, Kowloon, Hong Kong, P. R. China.

[c] High Magnetic Field Laboratory, Hefei Institutes of Physical Science, Chinese Academy of Sciences, Hefei, Anhui 230031, P. R. China

[d] School of Electronic Engineering and Intelligent Manufacturing, Anqing Normal University, Anqing, Anhui 246052, P. R. China

‡ These authors contributed equally to this work.

* Corresponding Author, E-mail: cqw@ustc.edu.cn

Experimental Section

Synthesis of V-NDC. The V-NDC MOF precursor was prepared with a modified hydrothermal method.[1] In a typical synthesis, 3 mmol anhydrous vanadium trichloride (VCl_3) and 1.5 mmol 1,4-naphthalenedicarboxylic acid (H_2NDC) were dissovled in 30 mL H_2O and vigorously stirred for for 1 h at room temperature. The mixed solution was then transferred into a Teflon-lined stainless steel autoclave (40 mL) and heated at 180 °C for 24 h. The earth-yellow powder was collected by centrifugation and washed with water and ethanol for three times each, and dried under vacuum overnight.

Synthesis of VO/C. The as-synthesized V-NDC precursor was placed in a quartz boat and annealed under inert atmosphere at 600 °C for 3 h to obtain the VO/C composite. The amorphous carbon was prepared by washing the VO/C composite with 3 M HNO_3 and dried under vacuum overnight.

Synthesis of KPB. The Prussian blue analogue $KFe[Fe(CN)_6]$ (denoted as KPB) was synthesized by a co-precipitation method according to a previous literature.[2]

Characterization. The morphology of the samples was characterized by scanning electron microscope (JEOL JSM-6700M and GeminiSEM 500). The powder XRD patterns were recorded with a Japan Rigaku D/MAX-γA X-ray diffractometer using Cu-Kα radiation. TEM images were acquired on a Hitachi H-7650 transmission electron microscope with an accelerating voltage of 100kV. The high-angle annular dark field scanning transmission electron microscopy (HAADF-STEM) and energy-dispersive X-ray (EDX) analyses were performed on a JEOL ARM-200F field-emission transmission electron microscope operating at 200 kV accelerating voltage. Raman spectra were collected on a LabRAM HR Raman spectrometer. TGA was carried out with a SDT Q600 (V20.9 Build 20) thermal analyzer system. XPS was conducted on a Thermo ESCALAB 250Xi X-ray photoelectron spectrometer instrument. The specific surface area was measured with the Brunauer-Emmett-Teller (BET) method using a Quantachrome

Instruments (version 4.01), while the pore volume and pore size were calculated according to the Barrett–Joyner–Halenda (BJH) formula applied to the adsorption branch.

Electrochemical measurements. The electrochemical performance was evaluated with CR2032 coin-type cells. The working electrode was prepared by mixing active materials (70 wt.%), acetylene black (20 wt.%) and polyvinylidene difluoride (10 wt.%) in N-methyl-2-pyrrolidone. Then the mixture was brush-coated on copper foil and dried under vacuum at 60 °C for 12 h. The mass loading of the working electrode was 0.7-0.8 mg cm^{-2}. Potassium metal was used as the counter/reference electrode and glass fiber (Whatman, GF/D) was used as the separator. The electrolyte was 1 M KFSI dissolved in a 1:1 (v:v) mixture of ethylene carbonate and diethyl carbonate. The cathode was fabricated in the same way on aluminum foil. The cathode-to-anode mass loading ratio was about 3:1. The cells were assembled in an argon-filled glovebox with both the moisture and the oxygen contents below 0.1 ppm. Galvanostatic charge/discharge measurements were performed on a battery test system (Neware CT-3008W) in a voltage range of 0.01-3.0 V (vs K^+/K) at room temperature. The cyclic voltammograms (CV) and electrochemical impedance spectroscopy (EIS) were tested on a CHI760E electrochemical workstation.

Computational methods. The calculations in this study were performed using density functional theory (DFT) as implemented in Vienna ab initio simulation package (VASP).[3] The projector augmented wave (PAW) method was applied to describe the interaction of electrons with the ionic cores.[4] Electron exchange-correlation was represented by the functional of Perdew, Burke and Ernzerhof (PBE) of generalized gradient approximation (GGA).[5] For all calculations, the cutoff of the energy for plane-wave basis was set to 400 eV. All structures were optimized with a convergence criterion of 1×10^{-5} eV for the energy and 0.01 eV/Å for the forces. Brillouin zone sampling was employed using a Monkhorst-Packing

grid with 3 × 3 × 1. And 5 × 5 × 1 K-point grid was used to calculate the density of states (DOS). The climbing-image nudged elastic band (CI-NEB) method was used to study the diffusion barrier of K ions.[6]

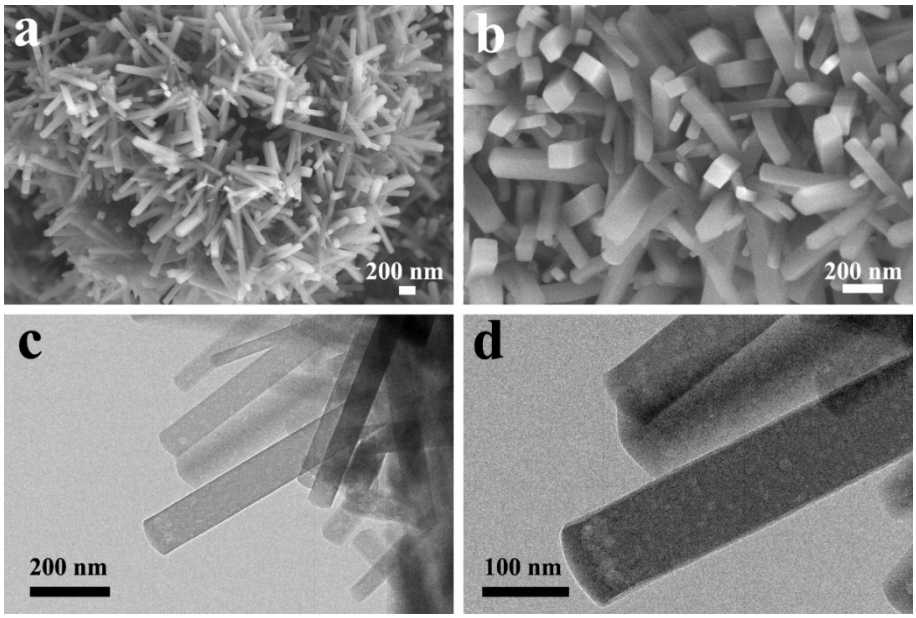

Fig. S1. (a, b) SEM and (c, d) TEM images of the as-synthesized V-NDC precursor.

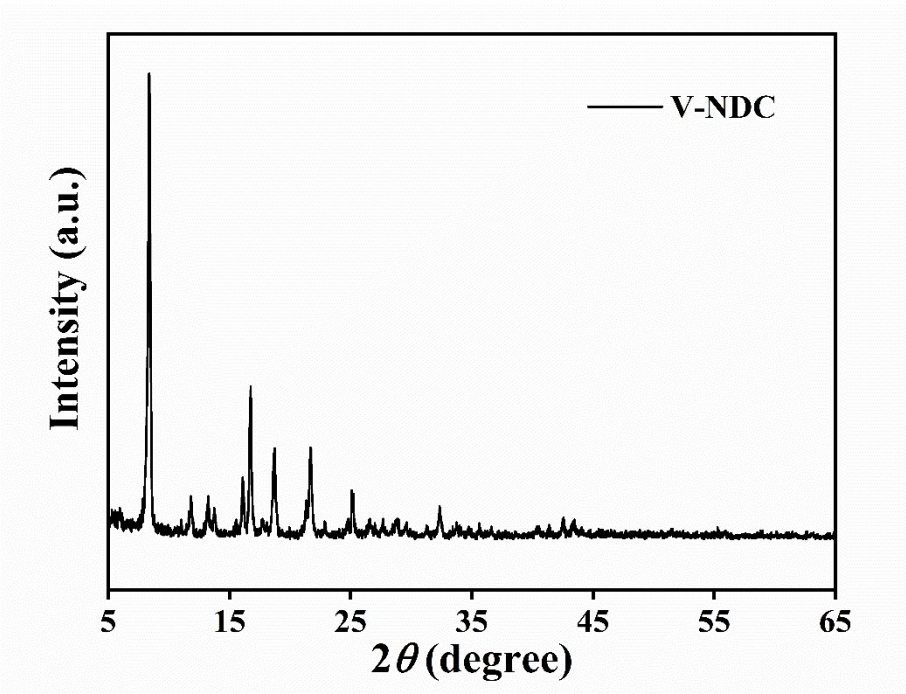

Fig. S2. XRD pattern of the as-synthesized V-NDC precursor.

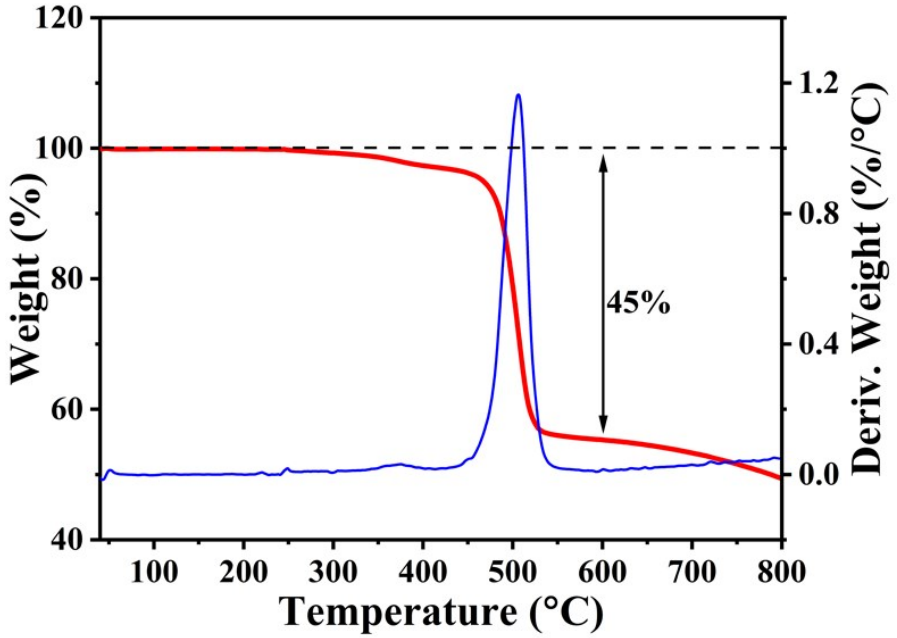

Fig. S3. TGA curve of the V-NDC precursor under inert atmosphere.

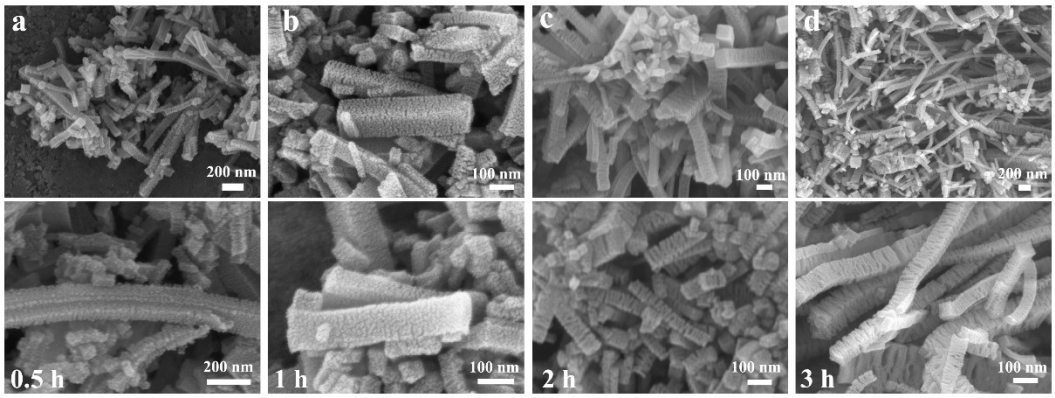

Fig. S4. Characterizations of the structural evolution of the V-NDC precursor after different time during the annealing process. (a) 0.5h; (b) 1h; (c) 2h; (d) 3h.

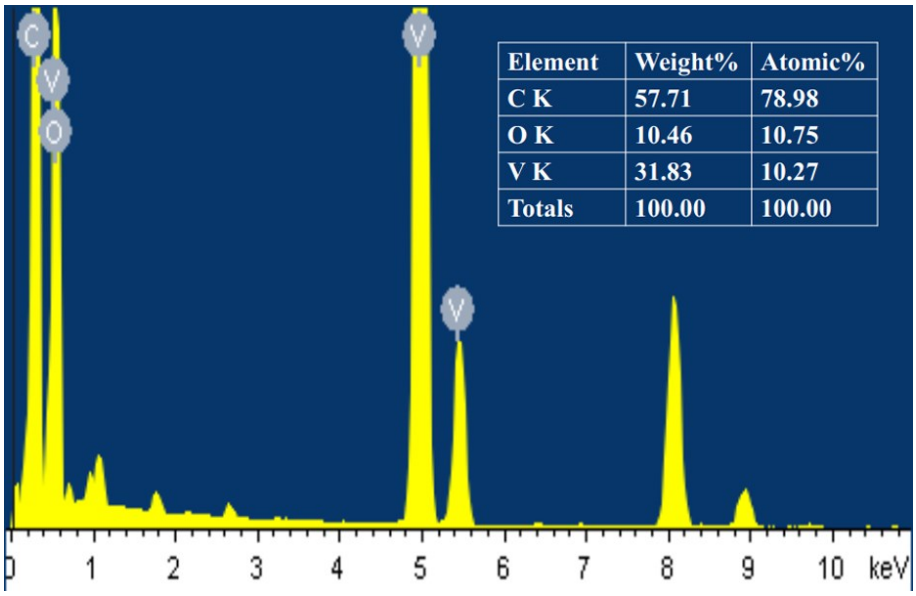

Element	Weight%	Atomic%
C K	57.71	78.98
O K	10.46	10.75
V K	31.83	10.27
Totals	100.00	100.00

Fig. S5. EDS elemental analysis of VO/C.

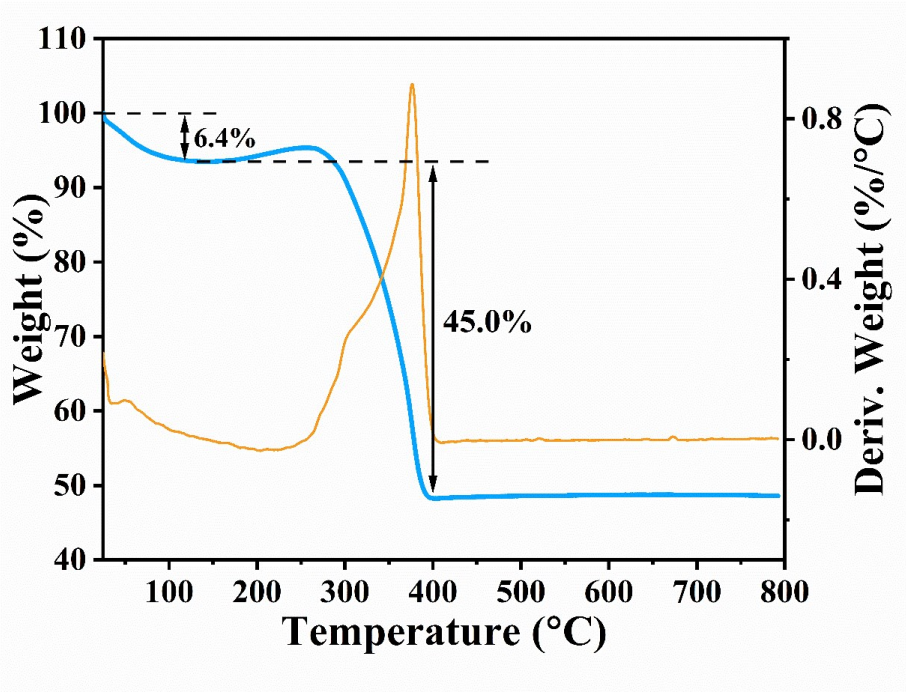

Fig. S6. TGA curve of VO/C in air.

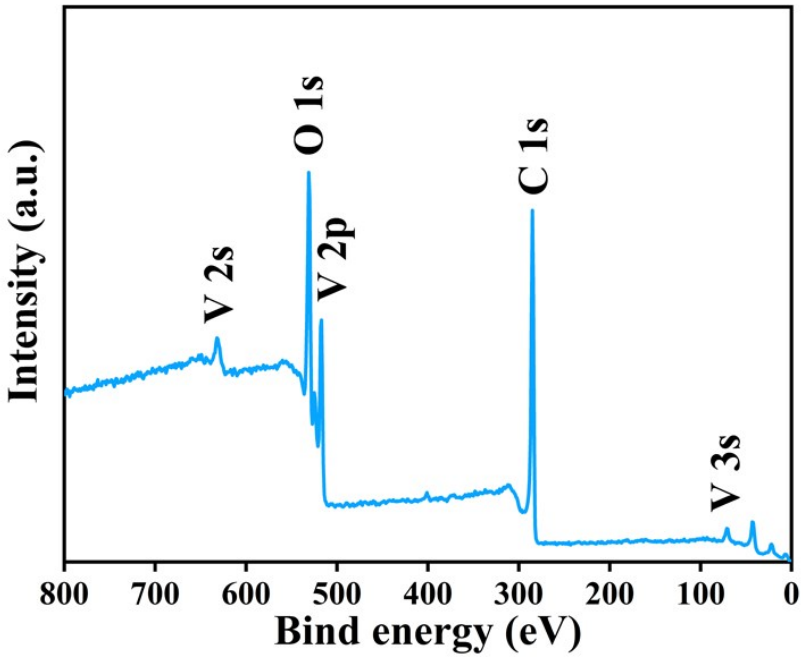

Fig. S7. XPS survey of the VO/C sample.

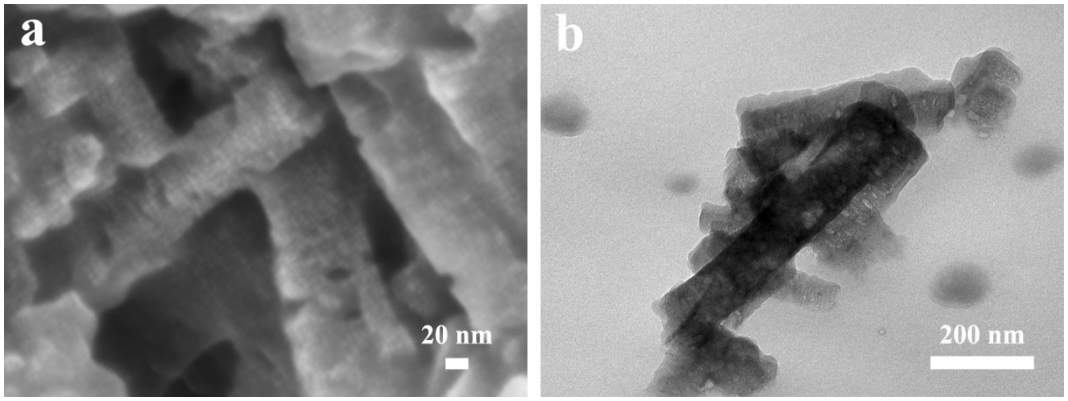

Fig. S8. (a) SEM and (b) TEM images of the VO/C electrode after 1000 cycles at a current density of 1 A g^{-1}.

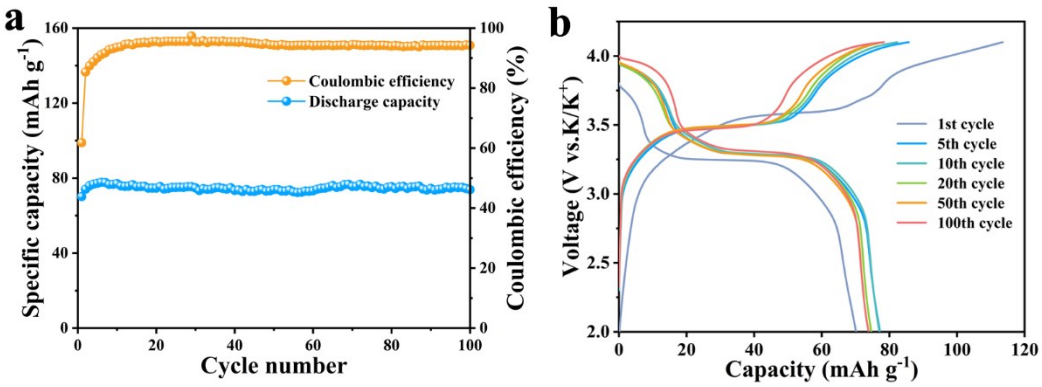

Fig. S9. The electrochemical performance of the KPB cathode in half-cell. (a) The cycling stability of KPB at 25 mA g^{-1} for 100 cycles in 2.0–4.1 V and (b) the corresponding charge/discharge curves.

Table S1. K-storage performance comparison of the VO/C electrode with previously reported metal oxides-based anodes and some other representative anodes for PIBs.

Anode materials	Cycling performances			Rate capability		Ref.
	Current density (A g^{-1})	Cycling number	Capacity (mA h g^{-1})	Current density (A g^{-1})	Capacity (mA h g^{-1})	
VO/C	**0.1 1**	**400 1000**	**345 241**	**1/2 10/15**	**244/218 133/104**	**This work**
Co_3O_4–Fe_2O_3/C	0.05	50	220	Not given		[7]
$Pb_3Nb_4O_{13}$ nanowires	0.05	1100	74.6	Not given		[8]
$K_{1.06}Mn_8O_{16}$/CNT	0.1	500	226.5	1	127.2	[9]
V_2O_3@PNCNFs	0.05	500	~230	1	134	[10]
HS-V_2O_3@C	0.1	500	330	5	79	[11]
SA-VO_2	0.05	50	288.3	2	141.4	[12]
T-Nb_2O_5	0.4	400	~76	1	74	[13]
MoO_2/3DPC	0.05 0.5	200 500	213 95	Not given		[14]
CuO nanoplates	0.2 1	60 100	276.7 206	1 2	206.8 163	[15]
Sb_2O_3-RGO	0.1 0.5	100 3300	309 201	1	172	[16]
TiO_2-carbon heterostructure	0.1 0.5	200 1200	197.5 132.8	1 2	114.6 97.3	[17]
MoO_2/rGO	0.05 0.5	200 500	218.9 104.2	0.5	176.4	[18]
SnO_2/SSM	0.05 1	100 200	351 128	1	125	[19]
Sb_2MoO_6/rGO	0.2 0.5	50 100	381 247	1	161	[20]
$FeVO_4$/C	0.3	2000	252.9	1 2	200.6 180.3	[21]
$K_{0.23}V_2O_5$	0.1	100	97.6	0.4	92	[22]

VN quantum dots	0.1 0.5	100 500	228 215	1 2	187 152	[23]
VS_2	0.1	60	410	2	100	[24]
VSe_2	0.2	200	335	2	169	[25]
$MoSe_2$/N-C	0.1	300	258	1 2	195 178	[26]
Graphite	0.14	50	100	0.28	80	[27]
Hard carbon	0.028	100	216	1.4	136	[28]
N-doped graphene	0.05 0.5	60 500	320 150	0.5	170	[29]
N-doped carbon nanofibers	0.025 2	100 4000	248 146	10 20	104 101	[30]
S/N@C	0.1	400	200	2 4	91.2 64	[31]
S/O co-doped carbon	0.05 1	100 2000	226.6 108.4	1	158	[32]
N/O dual-doped hard carbon	0.05 1.05	100 1100	230.6 130	3	118	[33]
Bi	0.8	300	321.6	1.2	321.9	[34]
Bi/rGO	0.05	50	290	0.5	235	[35]
Sn_4P_3/C	0.05	50	307.2	1	221.9	[36]
FeP@C	0.1	300	205	1 2	65 37	[37]

Table S2. The fitted impedances of VO/C and C.

Equivalent circuit model	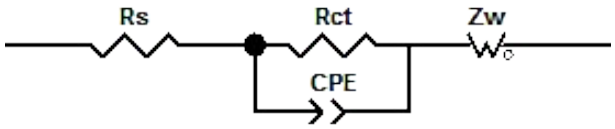	
Sample	**Rs (Ω)**	**Rct (Ω)**
VO/C	2.982	596.9
C	4.439	1751.0

In the equivalent circuit model, Rs represents solution resistance corresponding to the electrolyte and electrical contacts, and Rct represents charge transfer resistance. As shown in Table S2, VO/C possess a much lower Rct value than that of C, which demonstrates that the former has a better charge transfer kinetic. This is also consistent with the superior rate performance and cycling stability of the VO/C electrode.

References

[1] J. Reboul, K. Yoshida, S. Furukawa, S. Kitagawa, CrystEngComm 17 (2015) 323-330.

[2] G. He, L. F. Nazar, ACS Energy Lett. 2 (2017) 1122-1127.

[3] G. Kresse, J. Hafner, Phys. Rev. B 48 (1993) 13115-13118.

[4] G. Kresse, D. Joubert, Phys. Rev. B 59 (1999) 1758-1775.

[5] J. P. Perdew, K. Burke, M. Ernzerhof, Phys. Rev. Lett. 77 (1996) 3865-3868.

[6] G. Henkelman, B. P. Uberuaga, H. Jónsson, J. Chem. Phys. 113 (2000) 9901-9904.

[7] I. Sultana, M. M. Rahman, S. Mateti, V. G. Ahmadabadi, A. M. Glushenkov, Y. Chen, Nanoscale 9 (2017) 3646-3654.

[8] Z. Chen, X. Cheng, H. Yu, H. Zhu, R. Zheng, T. Liu, J. Zhang, M. Shui, J. Shu, Ceram. Int. 44 (2018) 17094-17101.

[9] S. Chong, Y. Wu, C. Liu, Y. Chen, S. Guo, Y. Liu, G. Cao, Nano Energy 54 (2018) 106-115.

[10] T. Jin, H. Li, Y. Li, L. Jiao, J. Chen, Nano Energy 50 (2018) 462-467.

[11] F. Chen, S. Wang, X.-D. He, J.-Y. Liao, Q. Hu, J.-M. Dong, C.-H. Chen, J. Mater. Chem. A 8 (2020) 13261-13266.

[12] Y. Li, Q. Zhang, Y. Yuan, H. Liu, C. Yang, Z. Lin, J. Lu, Adv. Energy Mater. 10 (2020) 2000717.

[13] N. Li, F. Zhang, Y. Tang, J. Mater. Chem. A 6 (2018) 17889-17895.

[14] S. Bao, S.-h. Luo, S.-x. Yan, Z.-y. Wang, Q. Wang, J. Feng, Y.-l. Wang, T.-f. Yi, Electrochim. Acta 307 (2019) 293-301.

[15] K. Cao, H. Liu, W. Li, Q. Han, Z. Zhang, K. Huang, Q. Jing, L. Jiao, Small 15 (2019) 1901775.

[16] J. Li, N. Zhuang, J. Xie, X. Li, W. Zhuo, H. Wang, J. B. Na, X. Li, Y. Yamauchi, W. Mai, Adv.

Energy Mater. 10 (2020) 1903455.

[17] Y. Li, C. Yang, F. Zheng, Q. Pan, Y. Liu, G. Wang, T. Liu, J. Hu, M. Liu, Nano Energy 59 (2019) 582-590.

[18] C. Liu, S. Luo, H. Huang, Y. Zhai, Z. Wang, ChemSusChem 12 (2019) 873-880.

[19] G. Suo, D. Li, L. Feng, X. Hou, Y. Yang, W. Wang, J. Electroanal. Chem. 833 (2019) 113-118.

[20] J. Wang, B. Wang, Z. Liu, L. Fan, Q. Zhang, H. Ding, L. Wang, H. Yang, X. Yu, B. Lu, Adv. Sci. 6 (2019) 1900904.

[21] X. Niu, Y. Zhang, L. Tan, Z. Yang, J. Yang, T. Liu, L. Zeng, Y. Zhu, L. Guo, Energy Storage Mater. 22 (2019) 160-167.

[22] C. Liu, S. Luo, H. Huang, Z. Wang, Q. Wang, Y. Zhang, Y. Liu, Y. Zhai, Z. Wang, J. Power Sources 389 (2018) 77-83.

[23] H. Y. Wu, Q. Y. Yu, C. Y. Lai, M. L. Qin, W. Wang, Z. W. Liu, C. Man, L. Y. Wang, B. R. Jia, X. H. Qu, Energy Storage Mater. 18 (2019) 43-50.

[24] J. Zhou, L. Wang, M. Yang, J. Wu, F. Chen, W. Huang, N. Han, H. Ye, F. Zhao, Y. Li, Y. Li, Adv. Mater. 29 (2017) 1702061.

[25] C. Yang, J. Feng, F. Lv, J. Zhou, C. Lin, K. Wang, Y. Zhang, Y. Yang, W. Wang, J. Li, S. Guo, Adv. Mater. 30 (2018) 1800036.

[26] J. Ge, L. Fan, J. Wang, Q. Zhang, Z. Liu, E. Zhang, Q. Liu, X. Yu, B. Lu, Adv. Energy Mater. 8 (2018) 1801477.

[27] Z. Jian, W. Luo, X. Ji, J. Am. Chem. Soc. 137 (2015) 11566-11569.

[28] Z. Jian, Z. Xing, C. Bommier, Z. Li, X. Ji, Adv. Energy Mater. 6 (2016) 1501874.

[29] Z. Ju, P. Li, G. Ma, Z. Xing, Q. Zhuang, Y. Qian, Energy Storage Mater. 11 (2018) 38-46.

[30] Y. Xu, C. Zhang, M. Zhou, Q. Fu, C. Zhao, M. Wu, Y. Lei, Nat. Commun. 9 (2018) 1720.

[31] A. Mahmood, S. Li, Z. Ali, H. Tabassum, B. Zhu, Z. Liang, W. Meng, W. Aftab, W. Guo, H. Zhang, M. Yousaf, S. Gao, R. Zou, Y. Zhao, Adv. Mater. 31 (2019) 1805430.

[32] M. Chen, W. Wang, X. Liang, S. Gong, J. Liu, Q. Wang, S. Guo, H. Yang, Adv. Energy Mater. 8 (2018) 1800171.

[33] J. Yang, Z. Ju, Y. Jiang, Z. Xing, B. Xi, J. Feng, S. Xiong, Adv. Mater. 30 (2018) 1700104.

[34] K. Lei, C. Wang, L. Liu, Y. Luo, C. Mu, F. Li, J. Chen, Angew. Chem. Int. Ed. 57 (2018) 4687-4691.

[35] Q. Zhang, J. Mao, W. K. Pang, T. Zheng, V. Sencadas, Y. Chen, Y. Liu, Z. Guo, Adv. Energy Mater. 8 (2018) 1703288.

[36] W. Zhang, J. Mao, S. Li, Z. Chen, Z. Guo, J. Am. Chem. Soc. 139 (2017) 3316-3319.

[37] F. Yang, H. Gao, J. Hao, S. Zhang, P. Li, Y. Liu, J. Chen, Z. Guo, Adv. Funct. Mater. 29 (2019) 1808291.